Asian Journal of Chemistry; Vol. 25, No. 1 (2013), 271-276

ASIAN JOURNAL OF CHEMISTRY

www.asianjournalofchemistry.co.in

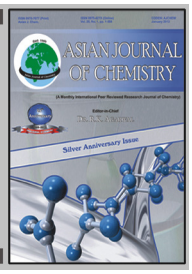

Microscopic Studies of Polyaniline-poly-*N*-isopropylacrylamide-*co*-acrylic acid/ Flyash Composites Containing Dodecylbenzene Sulfonic Acid

SHASHIDHAR[1,*], RAMPRASAD[1], C. BASAVARAJA[2] and T.K. VISHNUVARDHAN[3]

[1]Department of Chemistry, SDM College of Engineering and Technology, Dharwad-580 002, India
[2]Department of Chemistry, Inje University, Kimhae 621 749, South Korea
[3]Department of Chemistry, Acharya Institute of Technology, Bangalore-560 090, India

*Corresponding author: E-mail: nshashidharreddy@gmail.com

(*Received*: 31 October 2011; *Accepted*: 20 July 2012) AJC-11861

Polymer composites containing polyaniline-poly-*N*-isopropylacrylamide-*co*-acrylic acid (PAA)/flyash (FA) were synthesized by chemical polymerization of aniline in an aqueous solution containing dispersed poly-*N*-isopropylacrylamide-*co*-acrylic acid (PNA)/flyash (FA) in the presence of dodecylbenzene sulfonic acid using different wt % of flyash (5, 10, 20 and 30 %). The structure and morphology of the polymer matrix affected by the added were studied by atomic force microscope. The direct current electrical conductivity was studied as a function of flyash content in the temperature range of 293-483 K. The results show an increase in conductivity values as the temperature increases at a particular concentration of flyash. However, further increase in flyash causes a decrease in the conductivity.

Key Words: Dodecylbenzene sulfonic acid, Polyaniline-poly-*N*-isopropylacrylamide-*co*-acrylic acid/Flyash, Polymerization.

INTRODUCTION

In recent years, polyaniline (PANI) is doped with metal oxides to enhance physico-chemical properties that can substantially broaden the potential applications in various fields, especially in constructing electronic devices[1-3]. These composites have similar characteristics to those made by conventional semiconductors, with significant flexibility and processability[4-10]. Doping of these oxides into polyaniline is possible by electrochemical deposition, electroless precipitation, solution casting and vacuum deposition techniques[5-14].

Poly-*N*-isopropylacrylamide-*co*-acrylic acid or poly-*N*-isopropylacrylamide (PNIPAm) is one of the most interesting sensitive polymer microgels which have been extensively studied because its lower critical solution temperature (LCST) is close to room temperature. Pelton *et al.*[15] were the first to prepare stable PNIPAm particles by polymerizing *N*-isopropylacrylamide in the presence of polystyrene and polystyrene-butadiene latexes because PNIPAm can be dissolved easily by using a chelating agent that binds to the ions. Moreover, their size ranges typically from 50 nm to 5 μm. Recently, several types of colloids by silica, gold nanoparticles and carbon nanotubes have been used for surface-modification with PNIPAm by using the property of thermal response of PNIPAm in an aqueous medium[16]. The microgels such as PNIPAm possess several advantages over bulk gels, for example, small size and volume, high surface area, faster response to stimuli and high diffusivity.

A colloidal particle of dodecylbenzene sulfonic acid (DBSA) is known as a steric stabilizer and has a potential to be dispersed finely in an aqueous medium due to their small size. Polyaniline synthesized by any chemical method is usually amorphous in nature. The presence of poly-*N*-isopropylacrylamide-*co*-acrylic acid (PNA) and DBSA in solution state adsorbs most of aniline monomers onto their complex network. Introduction of acrylic acid (AA) groups in PNA is interesting since carboxy groups promote the adhesion to metal substrates[17,18]. Polymerization of aniline under these circumstances will help to improve the nature of interaction between polyaniline-metal particles. This is well supported by the result that the incorporation of DBSA in PANI/$PbTiO_3$ showed an intrinsic change in the crystallinity and conducting properties of polyaniline as compared to bare PANI/$PbTiO_3$ composites[19].

Recently, we have reported on the physico-chemical characteristics of the polymer composites containing polyaniline-poly-*N*-isopropylacrylamide-*co*-acrylic acid/alumina (PANI-PNA/Al_2O_3) which were synthesized by chemical polymerization of aniline in an aqueous solution containing dispersed PNA/Al_2O_3 in the presence of DBSA[20]. The composites show an improvement in the thermal stability and

crystallinity along with an enhancement in the chemical interaction between the polymer and alumina. However, the conductivity values decreased as the concentration of Al_2O_3 increases with increasing temperature. This may be attributed to the deceleration of the hopping process in the composites. In order to overcome the property we have incorporated flyash instead of alumina in the polymer matrix of PAA in a similar way in this study. The DC electrical conductivity was studied as a function of flyash concentration in the temperature range 293-483 K. The conductivity data indicates semiconducting behaviour similar to PANI-PNA/Al_2O_3 which increases with temperature for a particular concentration of flyash. However, further increase causes a decrease in conductivity values.

EXPERIMENTAL

Materials and synthesis of composites: AR grade NIPAAm, acrylic acid (AA), potassium persulfate (KPS), aniline, ammonium persulfate (APS) and *N,N'*-methylenebisacrylamide (MBA) were purchased from Sigma-Aldrich. Dodecylbenzene sulfonic acid (DBSA) and *N*-methyl-2-pyrrolidinone (NMP) were obtained from Junsei Chemical Co. A fine and pure flyash powder was collected from the Raichur Power Station, Raichur, India. The Cenosphere type flyash was grounded and sintered at 600 ºC to remove moisture content and some dust mpurities present. All solutions were prepared in aqueous media using deionized water.

Fig. 1 shows a model how polyaniline and flyash were incorporated into PNA microgels with the help of DBSA surfactant through the free emulsion polymerization method[20]. Synthesis of PNA was carried out using the equivalent grade NIPAAm (0.005 M), acrylic acid (0.003 M), MBA (0.002 M) and KPS (0.001 M) in 300 mL deionized water in a three-necked flask at 70 ºC under nitrogen atmosphere with vigorous stirring. In the case of composites, flyash powder was taken in a different (5, 10, 20 and 30) wt % with respect to the aniline concentration and was added to the above mixture. The obtained solution was cooled and aniline (0.05 M) and DBSA (0.025 M) were added slowly with constant stirring followed by a drop of ammonium persulfate solution at 0-5 ºC. The reaction was carried out for 7-8 h. The -COOH group of acrylic acid acts as a codopant in PNA microgels and helps to adsorb aniline monomers onto the PNA microgels. The addition of oxidant (ammonium persulfate) initiates the oxidative polymerization of polyaniline in the system. The forms of individual polyaniline particles which are not deposited into the microgel network will be included in the DBSA micelles. This shows how polyaniline is incorporating into the microgel structure and forming composites.

After then, the resulting precipitate was filtered and washed thoroughly with deionized water and acetone. And it was dried under vacuum for 24 h to achieve a constant weight. The powder was treated with a solution of sodium ethoxide (C_2H_5ONa) and ethanol and was magnetically stirred at room temperature for 12 h. Finally, the precipitate was filtered and washed repeatedly with ethanol and stored in a desiccator for 4 h at room temperature. Later 1-2 g of finely ground powder was taken and added to 30 mL of *N*-methyl-2-pyrrolidinone solution magnetically stirred for 24 h at room temperature.

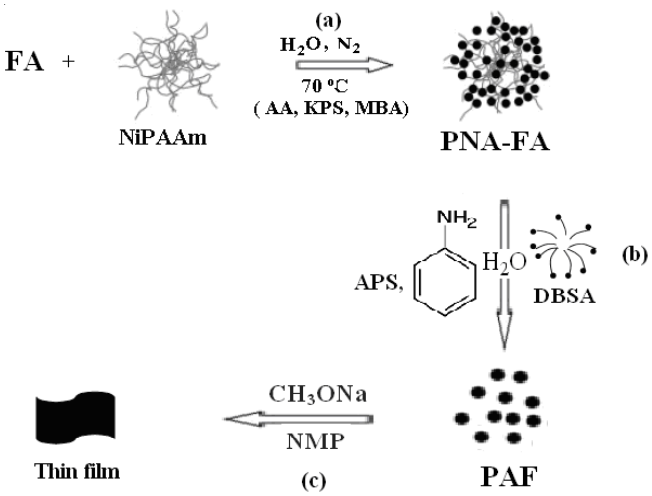

Fig. 1. Polymerization of PANI in the presence of PNA/flyash microgels (a) Incorporation of flyash into the PNA matrix. (b) Polymerization of aniline in the presence of DBSA and PAF. (c) Formation of PAF thin films

The concentrated solution was then placed into a Petri dish and the *N*-methyl-2-pyrrolidinone solvent was allowed to evaporate at 45 ºC for 48 h. The films with thickness of *ca.* 30 µm were placed in distilled water, followed by rinsing with ethanol and drying at room temperature for another 24 h. To obtain solvent-free films, the residual *N*-methyl-2-pyrrolidinone was removed by three cycles of doping using 1 M HCl solution for 18 h and de-doped by 0.1 M NH_4OH solution for another 18 h at room temperature. The resulting NMP-free composite films were cleaned in deionized water and were dried at room temperature for 24 h[21]. In the following sections the composites of PAA and flyash are abbreviated as PAF and the composites with 10, 20 and 30 % of flyash as PAF-10, PAF-20 and PAF-30, respectively.

The surface morphology of the composite films were investigated by using AFM which was performed by commercial Digital TESP7 VEECO at 25 ºC at a rate of 1 Hz for 1 µm and 500 nm. Thermal properties were obtained by TGA (Perkin-Elmer model TGA 7) in the range 30-700 ºC at 10 ºC/min in nitrogen atmosphere. The measurements of complex impedance were performed over a temperature range 298-533 K using impedance/gain-phase analyzer(Hewlett-Packard LF4194A) at 100 Hz. The parallel surfaces of pressed pellets, 1.5 mm × 1.3 mm, were coated with gold by means of vacuum evaporation and silver electrodes were placed on both surfaces with the help of silver paste to obtain better contact which acts as electrodes. The conductivity/resistivity values indicated here are the mean values taken by varying the temperatures with heating and cooling during the measurements.

RESULTS AND DISCUSSION

Surface morphology of the PAF composites by AFM: 2D and 3D images of 1mm scans and section plots of 1 µm scans for PAA interfaces formed using different flyash concentrations are indicated in Figs. 2-4. Fig. 2a shows the three dimensional image of PAA. The surface appears as fairly smooth and amorphous in the form of small and equally distributed narrow features repeated whole along the surface. The

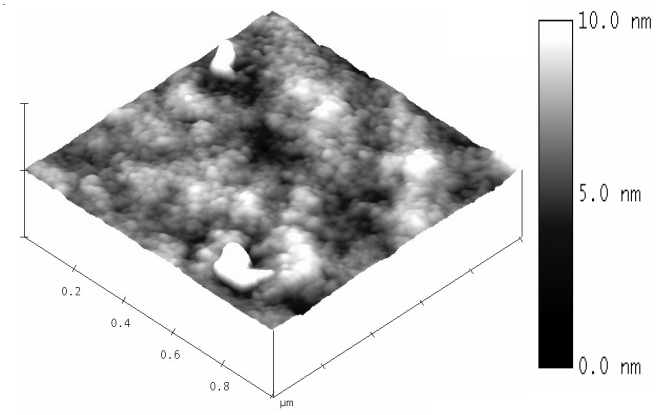

(a)

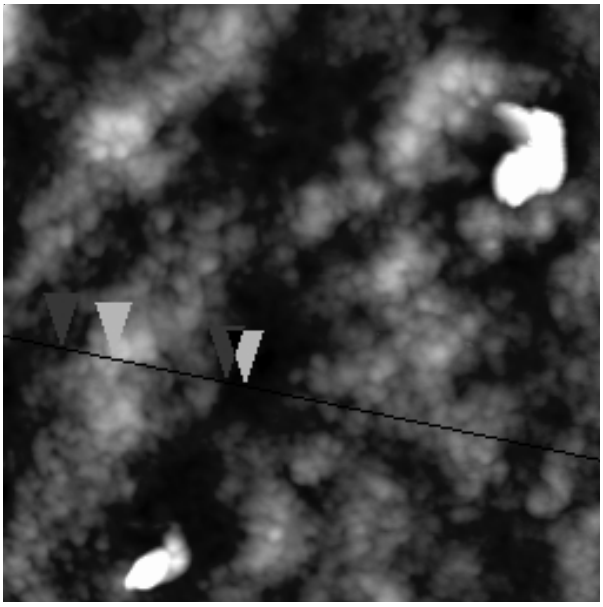

(b)

Fig. 2. AFM image for the PAA interfaces, (a) 3-D scanned images, (b) 2-D scanned images

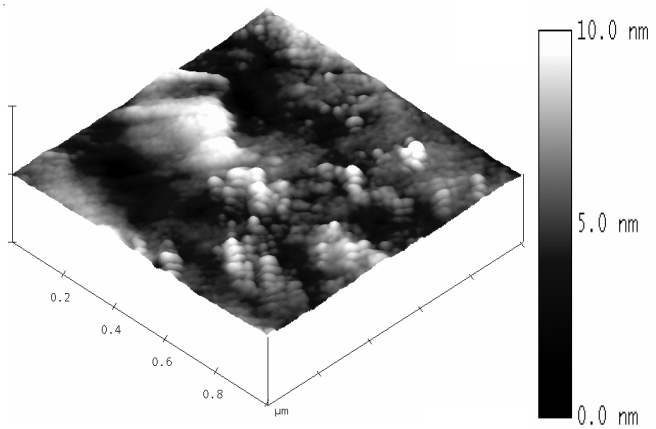

(a)

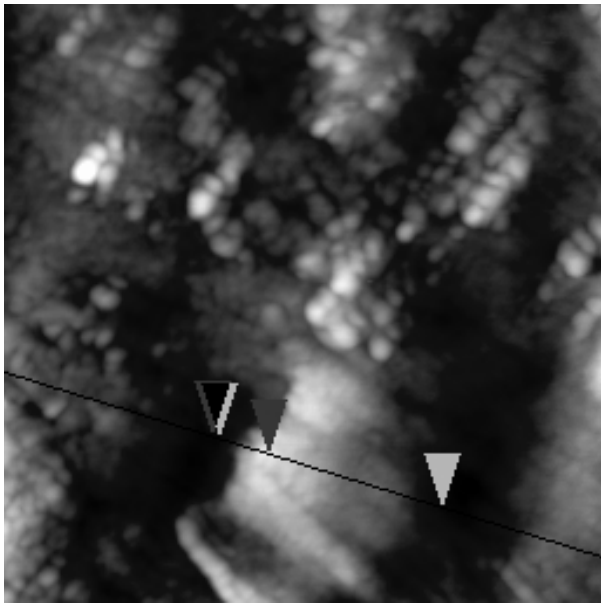

(b)

Fig. 3. AFM image for the PAF-10 interfaces, (a) 3-D scanned images, (b) 2-D scanned images

height of the features seems to be *ca.* 10 nm. This can be further evidenced by the 2D surface analysis which is indicated in Fig. 2b. Further the sectional analysis of the PAA shows that the diameter of these features is *ca.* 225 nm. Fig. 3a shows the three dimensional image of PAF-10 which indicates the disappearance of narrow features appeared in PAA due to the incorporation of flyash. The introduction of flyash makes the surface of PAA fairly rough with no change in the height as one can see from Fig. 3b. However the diameter of these features has changed to 390 nm. Further increase in the concentration of flyash has changed the surface more significantly along with the height as in Fig. 4a and 4b. The sectional analysis indicates the decrease in diameter of the features formed in the polymer as 265 nm. A comparison of the section plots shows flattening or broadening of surface features of the composite has been observed with an increase in the concentration of flyash. The nano-cavities formed in PAA are disappeared at higher concentration due to higher surface density of PAF films. Along with this the RMS roughness values of PAA, PAF-10 and PAF-30 interfaces are shown to increase with increasing flyash concentration in the polymer. The PAA has RMS roughness as 2.7 which increase to 3.6 for PAF-10 and 8.9 for PAF-30, respectively. Thus the surface uniformity in terms of distribution of features size is significantly modified by the introduction of flyash in PAA matrix.

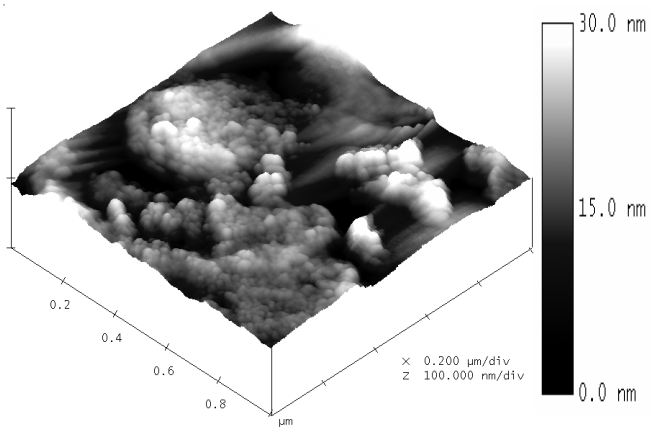

(a)

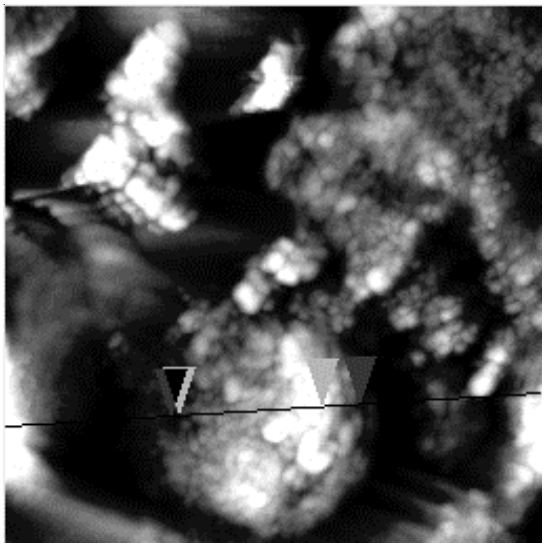

(b)

Fig. 4. AFM image for the PAF-30 interfaces, (a) 3-D scanned images, (b) 2-D scanned images

Thermal properties PAA and PAF composites: The TGA curves of PAA, PAF-10 and PAF-30 are shown in Fig. 5. These composites exhibit three steps of mass losses. The initial loss below 100 ºC is assigned to the gradual evaporation of moisture/PNA. The second around 250-500 ºC is due to the thermo-chemical decomposition of the chemically active organic materials at this range; DBSA mainly at 150-300 and the third is around 250-500 ºC. The mass loss for PAA, PAF-10 and PAF-30 are very slow under 500 ºC, which slightly increases with the increase in the content of flyash. Above the temperature, degradation proceeds rapidly. The third stage starts in the range of 500-600 ºC, which implies a complete decomposition of organic polymers leaving only the oxide particles whose degradation occurs at a higher temperature. PAA shows a residual weight of 36 % at 600 ºC, which increases after the introduction of flyash into PAA. The PAF-10 matrix shows a residual weight of 40 %, which subsequently increases to 45 % for the PAF-30 composite, which means the incorporation of flyash in the polymer matrix shows an increased thermal stability.

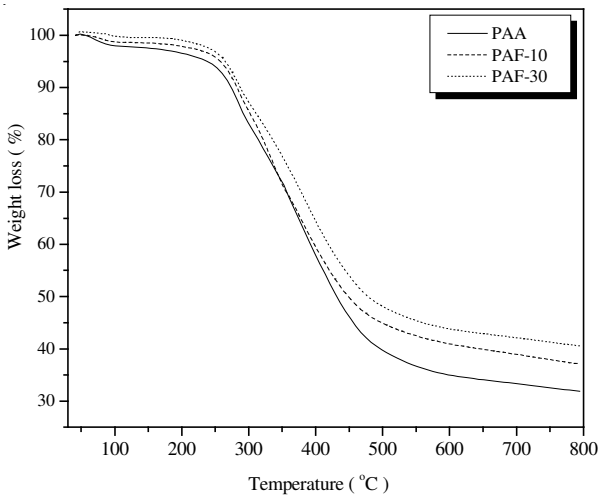

Fig. 5. TGA curve of PAA, PAF-10 and PAF-30 films recorded under N_2 atmosphere at a heating rate of 10 ºC/min

Transport properties PANI-PNA/flyash composites: Thermo-sensitive polymers such as PNIPAm and its derivatives like poly-*N*-isopropylacrylamide-*co*-acrylic acid (PNA) are well known for their properties relating with phase such as LCST, moisture sensitivity, dependence of electrical conductivity on humidity at different temperature, *etc*. Fig. 6 shows the variation of electrical resistance with temperature for PAA and PAF-10, PAF-20 and PAF-30. The behaviour is similar to a semiconducting material as the content of flyash is increased. The resistivity decreases for PAF-10 and PAF-20 while that of PAF-30 increases exponentially with temperature. The temperature coefficient of resistivity (TCR) was determined by the variation of the electrical resistivity with temperature using the relation:[21,22]

$$TCR = \left(\frac{1}{\rho(T_1)}\right)\left(\frac{\Delta\rho}{\Delta T}\right) \quad (1)$$

where $\Delta\rho = \rho(T_1) - \rho(T_2)$ and $\Delta T = T_2 - T_1$.

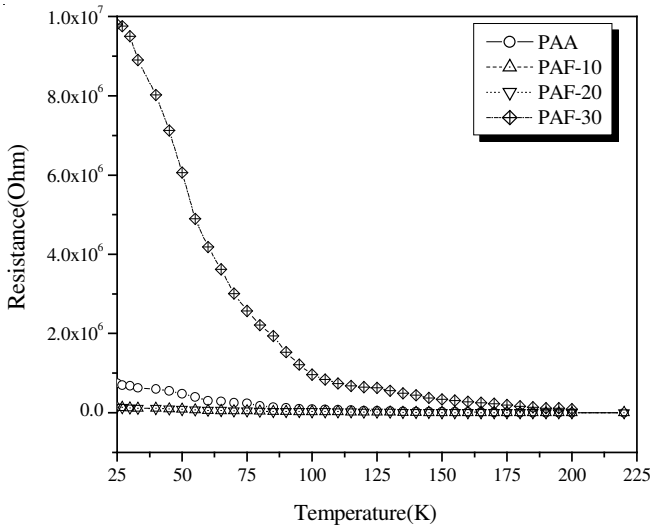

Fig. 6. Electrical resistance *versus* temperature for the composites PAA, PAF-10, PAF-20 and PAF-30

Table-1 shows calculated TCR values for different composites. The values are negative and they increase only for PAA in the range of temperatures as indicated. They decrease after the incorporation of flyash in the PAA matrix as one see the sets of values for PAF-10, PAF-20 and PAF-30 in the table. Similar to resistance, conductivity increases for the composites PAF-10 and PAF-20, decreases drastically for PAF-30.

TABLE-1
CALCULATED VALUES OF TEMPERATURE COEFFICIENT OF RESISTIVITY (TCR) OF PAA AND THE COMPOSITES PAF

Temperature range (K)	Temperature coefficient of resistivity (TCR)			
	PAA	PAF-10	PAF-20	PAF-30
298-348	-0.0123	-0.0133	-0.0134	-0.0147
348-408	-0.0137	-0.0110	-0.0116	-0.0134
408-448	-0.0171	-0.0185	-0.0153	-0.0150
448-488	-0.0197	-0.0088	-0.0136	-0.0117

The conducting polymer structure is typically aligned in the form of chains interspersed with regions where the chains

are disordered[23] and it is assumed that there are highly conducting islands in a sea of amorphous polymer. The nonmetallic temperature dependence of polyaniline doped by small molecular dopant (DBSA) causes the higher mobility of counterions at higher temperature which is caused by the mobility of counterions of DBSA at higher temperature. PAA shows a nonmetallic sign of conductivity and the temperature dependence, this shows an increase in conductivity with increasing temperature. This property may be attributed to the modification of bulk morphology of these composites. The decrease in conductivity of PAF-30 may be attributed to the disordering of polymeric chain in the composite due to flyash particles interspersed in the polymer matrix[11]. The relationship between the electrical conductivity and temperature was determined by the Arrhenius equation as given in eqn. 2 and the activation energies for conduction at various temperatures are shown in Table-2.

TABLE-2
CALCULATED VALUES OF ACTIVATION ENERGIES OF PAA AND THE COMPOSITES PAF USING eqn. 2

Temperature range (K)	Activation energy (E_a) k Cal/mol			
	PAA	PAF-10	PAF-20	PAF-30
298-323	2.54±0.35	5.56±0.25	14.15±0.24	6.78±0.20
323-473	15.96±0.43	16.99±0.15	19.05±0.29	17.76±0.21
473-533	16.673±0.26	14.193±0.25	21.03±0.17	18.809±0.27

Fig. 7 shows the logarithm of conductivity *versus* inverse value of temperature for PAA and PAF-10, PAF-20 and PAF-30. The decrease in conductivity in PAF-30 is the order of 10 as compared to PAA and 100 compared to PAF-10 and PAF-20. This behaviour is completely different from those of PANI-PNA/Al_2O_3 which showed three different conductivity regions in the form of small jerks (jump) due to the change in the mechanism of conduction[20]. The behaviour in the present case is due to the excess sufficient thermal energy to excite electrons only at the conduction band (thermal process). Such behaviour can be expressed by the Arrhenius equation[24]:

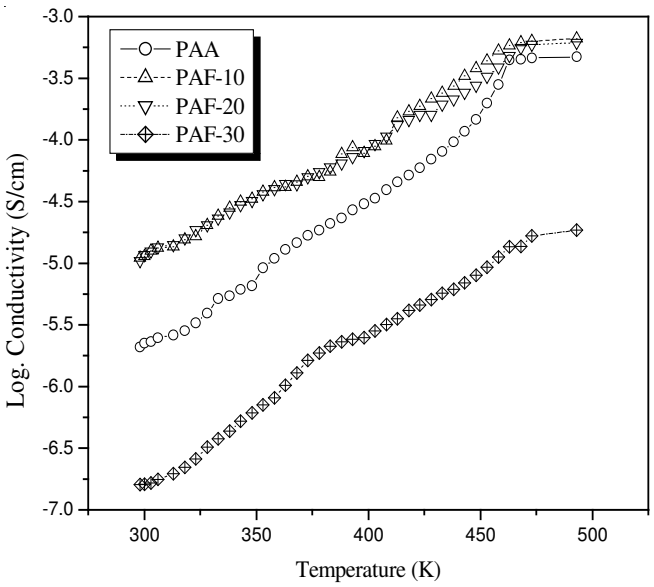

Fig. 7. Logarithm of conductivity *versus* temperature inverse for PAA, PAF-10, PAF-20 and PAF-30

$$\sigma = \sigma_0 \exp\left(\frac{-E_a}{k_B T}\right) \quad (2)$$

where s is the DC conductivity, σ_0 is a material constant which has units of conductivity, k_B is Boltzmann constant, T is absolute temperature and E_a is the activation energy. The increase in conductivity in case of PAF-10, PAF-20 is attributed to hopping process, where the excited electrons in this region lose their ability to jump to the conduction band with temperature[25]. Thus the electron attempts to find a state of similar energy by tunneling beyond its nearest neighbors to hop into more distant sites. This hopping leads to greater selection of the possible energy levels of the electrons. The behaviour of the DC conductivity in this region is called variable range hopping expressed in Mott's theory[25,26] as:

$$\sigma = \frac{\sigma_{02}}{T^{1/2}} \exp(-AT^{-1/4}) \quad (3)$$

where A and σ_{02} are material constants. The values of E_a were determined from the slopes of the fitted lines in Fig. 8 (best fit of Arrhenius curves) are indicated in Table-2 at different temperature ranges. These values showed the dependence of the thermal rate-process of electron transport within these temperature ranges. The activation energy is related to the energy barrier preventing polymer chain movement from one location to another. The strength of the interaction between the oxide and the polymer mainly depends on the property of the interface. The apparent activation energy showed a pronounced dependency on the flyash concentrations which increases with temperature. Fig. 8 presents the relation of log ($\sigma_v \times T^{1/2}$) *versus* $T^{-1/4}$ for three different composites. As we can see here also there is a drastic change is observed in case of PAF-30 which is like a straight line near zero value. Whereas in the case of PAA, PAF-10 and PAF-20, the values decrease from a higher value to a lower and PAA is at the lower side compared to PAF-10 and PAF-20. This observation is not consistent with the Mott's variable range of hopping process[24-27].

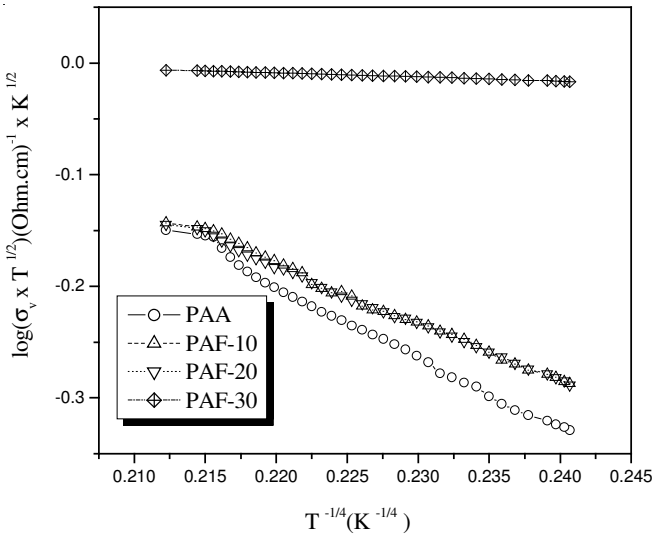

Fig. 8. log ($\sigma_v \times T^{1/2}$) *versus* $T^{-1/4}$ for PAA, PAF-10, PAF-20 and PAF-30

The trend in the behaviour of TCR in both PANI-PNA/Al_2O_3 and PAF are similar with a small change in the magnitude.

The values of activation energy decrease for PAF-10 and while these values increases for the composites of PAF-20 and PAF-30 as the temperature is increased. The energy of activation for the composites of PANI-PNA/Al_2O_3 increases in the middle as the temperature is increased (298-473 K) and further it decreases at higher temperature (473-533 K)[20]. The resistivity behaviour in both the types of composites was found to be ohmic and the electrical resistance of both the composites on temperature is similar to semiconducting behaviour with negative TCR. The electrical conductivity of PAF composites increases with temperature in all the composites as we increase the flyash content. When the conductivity values of PAA are compared with those of its composites, the conductivity of composites is increased by the increase of flyash content from 10 to 20 wt %. If the flyash content is increased to 30 then there is a decrease drastically. The increase in conductivity values in case of PAF-10 and PAF-20 can be due to the conformational changes which facilitates the hopping process between polymer chains further increase in flyash as in PAF-30 makes the hopping process difficult and hence resulted in reduction of conductivity.

Conclusion

In this paper, thermally stable ternary composites PAF were synthesized in the presence of DBSA by the oxidative polymerization of aniline with different wt % of flyash. These composites show temperature-dependent electrical properties and the effect on dielectric properties with increasing the contents of flyash is notable[21,28]. The conductivity data of the composites indicates that there is a barrier for the concentration of flyash above which it has a negative effect on the conducting properties of these composites. The composites are thermally stable with appreciable and stable temperature-dependent dc conductivity. The microgels containing flyash in PAA helps in the dispersion and polymerization of aniline. This helps the composite in improving the interaction of the oxide and polyaniline particles. Therefore some futuristic application may be expected such thermal and electrical behaviour from the fly ash filled polymer matrix composites and they will prove to be a promising material for future high technology industries at a lower cost.

ACKNOWLEDGEMENTS

This work was supported by Inje University research group. The authors thank to Director, RSIC-IIT, Madras and RSIC-CDRI, Lucknow for providing spectral facilities. Thanks are also due to Principal, SDM College of Engineering and Technology, Dharwad for providing the necessary laboratory facilities.

REFERENCES

1. C.Y. Lee, H.G. Song, K.S. Jang, E.J. Oh, A.J. Epstien and J. Joo, *Synth. Met.*, **102**, 1346 (1999).
2. H.L. Wang, A.G. MacDiarmid, Y.Z. Wang, D.D. Gebler and A.J. Epstein, *Synth. Met.*, **78**, 33 (1996).
3. Y.Z. Wang, D.D. Gebler, L.B. Lin, J.W. Blatchford, S.W. Jessen, H.L. Wang and A. Epstein, *J. Appl. Phys. Lett.*, **68**, 894 (1996).
4. A. Gok, M. Omastova and J. Prokes, *Eur. Polym. J.*, **43**, 2471 (2007).
5. K.G. Neoh, T.T. Young, N.T. Looi, E.T. Kang and K.L. Tan, *Chem. Mater.*, **9**, 2906 (1997).
6. J. Wang, K.G. Neoh and E.T. Kang, *J. Colloid. Interf. Sci.*, **239**, 78 (2000).
7. Y. Xu, L. Dai, J. Chen, J.Y. Gal and H. Wu, *Eur. Polym. J.*, **43**, 2072 (2007).
8. C. Basavaraja, Y. Veeranagouda, L. Kyoung, R. Pierson, M. Revanasiddappa and D.S. Huh, *Bull. Korean Chem. Soc.*, **29**, 2423 (2008).
9. K.H. Wu, C.M. Chao, C.H. Liu and T.C. Chang, *Corr. Sci.*, **49**, 3001 (2007).
10. S.A. Chen, K.R. Chung, C.I. Chao and H.T. Lee, *Synth. Met.*, **82**, 207 (1996).
11. S.L. Lim, K.L. Tan and E.T. Kang, *Langmuir*, **14**, 5305 (1998).
12. C.P. Wong and S.B. Raja, *J. Appl. Polym. Sci.*, **74**, 3396 (1999).
13. Y. Haba, E. Segal, M. Narkis, G.I. Titleman and A. Siegmann, *Synth. Met.*, **110**, 189 (2000).
14. T.C.K. Yang, S.H.Y. Tsai, S.F. Wang and C.C. Juan, *Compos. Sci. Technol.*, **62**, 655 (2002).
15. R.H. Pelton and P. Chibante, *Colloids Surf.*, **20**, 247 (1986).
16. R.C. Silva, L. Arizmendi, M.D. Angel and J.R. Gracia, *Langmuir*, **23**, 8 (2007).
17. B.C. Kim, G.M. Spinks, C.O. Too, G.G. Wallace, Y.H. Bae and N. Ogata, *React. Funct. Polym.*, **44**, 245 (2000).
18. R. Sinha and U. Dayal, Geoenvironmental Design Practices for Flyash Disposal and Utilization, Allied Publishers, New Delhi (2002).
19. C. Basavaraja, R. Pierson and D.S. Huh, *J. App. Polym. Sci.*, **108**, 1070 (2008).
20. C. Basavaraja, R. Pierson, T.K. Vishnuvardhan and D.S. Huh, *Eur. Polym. J.*, **44**, 1556 (2008).
21. H.L. Hwang, C.Y. Sun, C.Y. Leu, C.L. Cheng and C.C. Tu, *Rev. Phys. Appl.*, 745 (1978).
22. A.B. Kaiser, *Adv. Mater.*, **13**, 927 (2001).
23. H.M. Rosenberg, Low Temperature Solid State Physics, Oxford University Press, U.K. (2000).
24. N.F. Mott and E.A. Davis, Electronic Process in Non-Crystalline Materials, Glarndon Press, Oxford (1971).
25. Z.X. Zhou, G. Cao, S. McCall, J.E. Grow, R.P. Guertin, C.H. Mielke and D.G. Rgckel, *Philios. Magaz. B*, **82**, 1401 (2002).
26. S.F. Yasin, A.M. Zihlif and A. Ragosta, *J. Mater. Sci.*, **16**, 63 (2005).
27. S.C. Raghavendra, S. Khasim, M. Revanasiddappa, M.V.N. Ambika Prasad and A.B. Kulkarni, *Bull. Mater. Sci.*, **26**, 733 (2003).
28. C. Basavaraja, R. Pierson, T.K. Vishnuvardhan and D.S. Huh, *Bull. Korean Chem. Soc.*, **29**, 1669 (2008).